\



Electron-impact ionization cross section calculations for lithium-like ions

Guo-Jie Bian(卞国杰), Jyh-Ching Chang(张稚卿), Keh-Ning Huang(黄克宁), Chen-Sheng Wu(武晨晟), Yong-Jun Cheng(程勇军), Kai Wang(王凯), and Yong Wu(吴勇)

Citation: Chin. Phys. B, 2022, 31 (**1**): 013401. DOI: 10.1088/1674-1056/ac229e
Journal homepage: http://cpb.iphy.ac.cn; http://iopscience.iop.org/cpb

What follows is a list of articles you may be interested in

Charge transfer in low-energy collisions ofBe^{3+} and B^{4+} ions with He

Kun Wang(王堃), Yi-Zhi Qu(屈一至), Chun-Hua Liu(刘春华), Ling Liu(刘玲), Yong Wu(吴勇), H P Liebermann, Robert J. Buenker

Chin. Phys. B, 2020, 29 (**9**): 093401. DOI: 10.1088/1674-1056/aba276

Positronium formation for positron scattering from metastable hydrogen

Lin Lin(林蔺), Hong-Nian Wang(汪宏年), Li-Guang Jiao(焦利光)

Chin. Phys. B, 2017, 26 (**3**): 033401. DOI: 10.1088/1674-1056/26/3/033401

Influence of electron correlations on double-capture process in proton helium collisions

Hoda Ghavaminia, Ebrahim Ghanbari-Adivi

Chin. Phys. B, 2015, 24 (**7**): 073401. DOI: 10.1088/1674-1056/24/7/073401

Formation of hydrogen atom in 2s state in proton-sodium inelastic scattering

Sabbah A. Elkilany

Chin. Phys. B, 2015, 24 (**3**): 033402. DOI: 10.1088/1674-1056/24/3/033402

Projectile angular-differential cross sections for single electron transfer in fast He^{+}-He collisions

Ebrahim Ghanbari-Adivi, Hoda Ghavaminia

Chin. Phys. B, 2015, 24 (**3**): 033401. DOI: 10.1088/1674-1056/24/3/033401

Electron-impact ionization cross section calculations for lithium-like ions

Guo-Jie Bian(卞国杰)[1], Jyh-Ching Chang(张稚卿)[2] Ke-Ning Huang(黄克宁)[3], Chen-Sheng Wu(武晨晟)[1,†], Yong-Jun Cheng(程勇军)[4], Kai Wang(王凯)[5], and Yong Wu(吴勇)[1,6]

[1] *National Key Laboratory of Computational Physics, Institute of Applied Physics and Computational Mathematics, Beijing* 100088, *China*
[2] *Department of Physics, National Tsing Hua University, Hsinchu* 300, *China*
[3] *Institute of Atomic and Molecular Physics, Sichuan University, Chengdu* 610065, *China*
[4] *School of Physics and Information Technology, Shaanxi Normal University, Xi'an* 710119, *China*
[5] *Hebei Key Laboratory of Optic-electronic Information and Materials, The College of Physics Science and Technology, Hebei University, Baoding* 071002, *China*
[6] *HEDPS, Center for Applied Physics and Technology, and College of Engineering, Peking University, Beijing* 100871, *China*

(Received 6 July 2021; revised manuscript received 25 August 2021; accepted manuscript online 1 September 2021)

The electron-impact ionization of lithium-like ions C^{3+}, N^{4+}, O^{5+}, Ne^{7+}, and Fe^{23+} is studied using a combination of two-potential distorted-wave and R-matrix methods with a relativistic correction. Total cross sections are computed for incident energies from 1 to 10 times of ionization energy and better agreements with the experimental results are obtained in comparison with the theoretical data available. It is found that the indirect ionization processes become significant for the incident energy larger than about four times of the ionization energy. Contributions from the exchange effects along the isoelectronic sequence are also discussed and found to be important. The present method can be used to obtain systematic ionization cross sections for highly charged ions across a wide incident energy range.

Keywords: total cross sections, electron-impact ionization, excitation-autoionization, distorted-wave

PACS: 34.50.Fa, 34.80.Dp **DOI:** 10.1088/1674-1056/ac229e

1. Introduction

Electron-impact ionization is an important physical process in plasma environment. Nonequilibrium plasma simulations, such as magnetic confinement fusion, inertial confinement fusion, and astrophysics, require a large amount of data on cross sections of electron-impact ionization, in which ionization cross sections directly affect the charge transfer and energy transport of the plasma state.[1–6] A great deal of attention has been paid to the electron-impact ionization for lithium isoelectronic sequence due to the K–L excitation-autoionization process, which plays an important role in ionization dynamics.[7,8] Although much work has been devoted to improving the theory of electron-impact ionization, there are still discrepancies between theoretical predictions and experimental data for some members of the sequence.[9,10] Therefore, it is of vital importance to investigate behavior of electron-impact ionization along the isoelectronic sequence.

Experimentally, the modulated crossed-beam technique is commonly used in measurements of electron-impact ionization. Lithium isoelectronic sequence has been extensively investigated in low Z ions. Absolute cross sections have been measured for Be^{+}, B^{2+}, C^{3+}, N^{4+}, O^{5+}, and Ne^{7+} ions[7,11–17] in the energy range of 18–2000 eV. Wong *et al.*[18] measured cross sections for Ti^{19+}, V^{20+}, Cr^{21+}, Mn^{22+}, and Fe^{23+} ions at approximately 2.3 times ionization energy with typical uncertainties of 10%. Moreover, Ba^{53+} ion was measured at 22 keV,[19] and U^{89+} ion was also be measured.[20]

Theoretically, extensive calculations have been performed with various methods. The most commonly used method for direct ionization is the Coulomb–Born approximation,[21] in which the continuum electrons are regarded as Coulomb or distorted waves. Younger[22,23] introduced several applications of the Coulomb–Born and distorted-wave approximations, which produced results for hydrogen-, helium- and lithium-like ions. However, performance of the Coulomb–Born method is poor and, in many cases, it overestimates total cross sections. The electron exchange in transition matrix elements and Coulomb distortion waves are observed to be vital. Jakubowicz and Moores[9] discussed the Coulomb–Born exchange and distorted-wave exchange approximations, which solved the problems in the inclusion of exchange for the positive ions. When the indirect process is dominant, the close-coupling method is considered to be an effective prescription to describe the quasi-bound states of the target ion.[9] Fursa and Bray[24] presented the electron-helium scattering with convergent close-coupling formulations. This method requires numerous computations and applies only to a system with few valence electrons. The initial and final states of electron-impact ionization process for neutral helium were studied in the R-matrix basis,[25] which is

†Corresponding author. E-mail: 251538424@qq.com

© 2022 Chinese Physical Society and IOP Publishing Ltd

a combined distorted-wave and close-coupling approach. A special feature of this method is the consistency of the initial bound state and the final continuum state of the ions. Furthermore, the R-matrix method, which is independent of the energy of the scattered electrons in the inner region, was extended to the electron-impact ionization of Ne^{7+}.[10]

In recent years, the two-potential distorted-wave (TPDW) approximation, which uses different asymptotic charges for the distorting potential to study the mutual screening of the faster and slower electrons, has been developed and widely used in the calculation of electron-, positron-, and proton-impact ionizations of hydrogen-, helium-, and beryllium-like ions.[26–34] Compared with other theoretical and experimental data, generally more reliable results are obtained in these works.

In this study, the ionization cross sections of C^{3+}, N^{4+}, O^{5+}, Ne^{7+}, and Fe^{23+} ions are computed using the TPDW approximation along with the R-matrix method. TPDW calculations are performed using different sets of distorting potential models, which consider the exchange interactions between scattered and bound electrons. This technique can generate accurate wavefunctions for the initial and continuum states composed of the ejected electron. The indirect ionization processes become non-negligible in higher incident energies, and the R-matrix code[35,36] is applied to obtain the excitation-autoionization cross sections. A brief review of the general theory for electron-impact ionization is presented in Section 2. Numerical results and discussions are given in Section 3, and the conclusion is provided in Section 4.

2. Theory

The total cross sections of electron-impact ionization of lithium-like ions are predicted by the two-potential distorted-wave method and the R-matrix calculation, where both the direct ionization and excitation-autoionization process are included. The helicity eigenstate, linear momentum, and energy of the incident electron are denoted by $|\boldsymbol{k}_{\rm i}\boldsymbol{\mu}_{\rm i}\rangle$, $\boldsymbol{k}_{\rm i}$, $E_{\rm i}$, respectively. After the collision, two outgoing electrons are described by $\left(\boldsymbol{k}_{\rm p}E_{\rm p}\boldsymbol{\mu}_{\rm p}\right)$ and $(\boldsymbol{k}_{\rm s}E_{\rm s}\boldsymbol{\mu}_{\rm s})$. Then according to the energy conservation law, we have

$$E_{\rm i}+E_{\rm b}=E_{\rm p}+E_{\rm s}, \tag{1}$$

where $E_{\rm b}$ represents the energy of bound electron. By integrating over the triple-differential cross section equation,[26] the single-differential cross section is calculated as

$$\begin{aligned}\frac{{\rm d}\sigma}{{\rm d}E_{\rm s}} &= \frac{(2\pi)^4}{c^6}\left[\frac{k_{\rm p}E_{\rm p}k_{\rm s}E_{\rm s}E_{\rm i}}{k_{\rm i}}\right]\int {\rm d}\Omega_{\rm p}\int {\rm d}\Omega_{\rm s}\sum_{(fi)}\left|T_{fi}\right|^2\\ &= \frac{2\pi^3}{k_{\rm i}^2(2J_0+1)}\sum_{\alpha}d_{\alpha},\end{aligned} \tag{2}$$

where J_0 is the total angular momentum of the target, and T_{fi} is the appropriate transition amplitude. The real amplitude d_α is defined by the reduced matrix element of the partial-wave amplitude in channel α,

$$\begin{aligned}d_\alpha\exp({\rm i}\delta_\alpha) &= {\rm i}^{I_{\rm i}-(I_{\rm p}+I_{\rm s})}\exp\left[{\rm i}(\sigma_{\kappa_{\rm p}}+\sigma_{\kappa_{\rm s}})\right]\\ &\quad\times\left\langle\alpha^-\left[J_\alpha(j_{\rm p}j_{\rm s})j\right]J\,\|H_I\|\,(j_{\rm b}j_{\rm i})J\right\rangle,\end{aligned} \tag{3}$$

where $\sigma_{\kappa_{\rm p}}$ and $\sigma_{\kappa_{\rm s}}$ are the Coulomb phase shifts of the two outing electrons, the index i refers to the incident electron, J_α and J are the total angular momentum of the residual ion and of the entire collision complex, and $H_{\rm I}$ is the appropriate interaction Hamiltonian.

The direct-ionization cross sections can be calculated as

$$\sigma=\int_{c^2}^{(E_{\rm i}+E_{\rm b})}\frac{{\rm d}\sigma}{{\rm d}E_{\rm s}}{\rm d}E_{\rm s}. \tag{4}$$

For electron-impact ionization of Li-like ions, the total Hamiltonian $H^{\rm (Li)}$ in atomic units can be split into the unperturbed part K_i and the interaction potential part V_i,

$$\begin{aligned}K_i &= \sum_{i=1}^{4}\left(c\alpha_i\cdot\boldsymbol{p}_i+c^2\beta_i\right)\\ &\quad-\frac{Z}{r_2}-\frac{Z}{r_3}-\frac{Z}{r_4}+\frac{1}{r_{23}}+\frac{1}{r_{24}}+\frac{1}{r_{34}},\end{aligned} \tag{5}$$

$$V_i = -\frac{Z}{r_1}+\frac{1}{r_{12}}+\frac{1}{r_{13}}+\frac{1}{r_{14}}. \tag{6}$$

Here, α_i and β_i are the Dirac 4×4 matrices, and $\boldsymbol{p}_i$ represents the momentum operator. Before the collision, subscript 1 represents the incident electron, and $i=2$, 3, 4 are the indices for bounded electrons. According to two-potential distorted-wave formulation, the potential V_i is separated into the distorting potential U_i and the residual potential W_i. They are defined as

$$U_i=-\frac{Z}{r_1}+v_i(r_1), \tag{7}$$

$$W_i=\sum_{i=2}^{4}\frac{1}{r_{1i}}-v_i(r_1), \tag{8}$$

where $v_i(r_1)$ is the effective potential. In the prior form, the transition amplitude can be reformulated exactly to the form

$$T_{fi}=\left\langle\Psi_f^{(-)}\,|W_i|\,\psi_i^{(+)}\right\rangle. \tag{9}$$

Here, the wave functions $\Psi_f^{(-)}$ and $\psi_i^{(+)}$ are eigenfunctions of $H^{\rm (Li)}$ and K_i+U_i with the incoming-wave and the outgoing-wave boundary conditions, respectively. The transition amplitude is not dependent on the choice of potential U_i, as long as the wave function is sufficiently accurate. In the present calculation, we choose a reasonable distorting potential U_i to make the disturbed effects of W_i as small as possible.

In our numerical calculation, the transition amplitude can be antisymmetrized following the general process of dealing with exchange effects in the scattering process. The final state

$\Psi_f^{(-)}$ and initial state $\psi_i^{(+)}$ will be evaluated as the semisymmetrized wave functions $\phi_f^{(-)}$ and $\phi_i^{(+)}$, respectively. The detailed description can be found in Ref. [34]. The matrix element in Eq. (9) by full antisymmetrization can be rewritten as

$$T_{fi} = D_{fi} + R_{fi} + C_{fi}, \tag{10}$$

$$D_{fi} = \left\langle (1-2Q_{23})\,\phi_f^{(-)}\,|W_i|\,\phi_i^{(+)} \right\rangle, \tag{11}$$

$$R_{fi} = -\left\langle (1-2Q_{23})\,Q_{12}\phi_f^{(-)}\,|W_i|\,\phi_i^{(+)} \right\rangle, \tag{12}$$

$$C_{fi} = -2\left\langle (1-Q_{23}-Q_{24})\,Q_{13}\phi_f^{(-)}\,|W_i|\,\phi_i^{(+)} \right\rangle. \tag{13}$$

Here, D_{fi} denotes the direct term, in which the incident electron becomes the faster electron after the collision. R_{fi} is the interchange term, in which the incident electron becomes the slower electron, and the bound 2s electron becomes the faster one. C_{fi} is the capture part, in which the incident electron becomes an 1s electron, and two bound electrons are knocked out. Q_{ij} represents the exchange operator of particle. The distorted wave $\chi_i^{(+)}$ of the incident electron with the outgoing-wave boundary condition can be solved from the equation

$$\left[c\boldsymbol{\alpha}_1\cdot\boldsymbol{p}_1 + c^2\beta_1 + U_i - E_i\right]\chi_i^{(+)}(\boldsymbol{r}_1) = 0, \tag{14}$$

For a lithium-like ion target in ground state configuration ($1s^2 2s$), the average screened potential $v_i(r_1)$ in U_i is defined as

$$v_i(r_1) = 2\left\langle \varphi_{1s}(\boldsymbol{r}_3)\left|\frac{1}{r_{13}}\right|\varphi_{1s}(\boldsymbol{r}_3)\right\rangle + \left\langle \varphi_{2s}(\boldsymbol{r}_2)\left|\frac{1}{r_{12}}\right|\varphi_{2s}(\boldsymbol{r}_2)\right\rangle. \tag{15}$$

Wave functions $\chi_{\rm p}^{(-)}$ and $\chi_{\rm s}^{(-)}$ of the outgoing electrons satisfy the equation with distorting potentials $U_{\rm p}$ and $U_{\rm s}$, respectively,

$$\left[c\boldsymbol{\alpha}_1\cdot\boldsymbol{p}_1 + c^2\beta_1 + U_{\rm p} - E_{\rm p}\right]\chi_{\rm p}^{(-)}(\boldsymbol{r}_1) = 0, \tag{16}$$

$$\left[c\boldsymbol{\alpha}_1\cdot\boldsymbol{p}_1 + c^2\beta_1 + U_{\rm s} - E_{\rm s}\right]\chi_{\rm s}^{(-)}(\boldsymbol{r}_2) = 0. \tag{17}$$

The distorting potentials can be approximated as Coulomb potential from the nuclei and the average screened potential, corresponding to the asymptotic charges $Z_{\rm p}$ and $Z_{\rm s}$. In this work, three models of distorting potential are applied in the calculation, and some information of these potentials is listed in Table 1. Models TPDW00 and TPDW11 are two extreme models for the electron-impact ionization process. In model TPDW00, the scattered electrons are completely screened from each other, so they experience the same distorting potential as the incident electron. In model TPDW11, it is completely free from the mutual screening effects by scattered electrons, thus both outgoing electrons are only affected by the bound electrons and the nucleus. The model TPDW01 is closer to the real scene, where the faster electron is completely screened by the slower electron in the asymptotic region, so that the faster electron is affected by the asymptotic charge of $Z-3$, and the slower electron is affected by the asymptotic charge of $Z-2$. The average screened potential due to the residual electrons of helium-like ions in $U_{\rm p}$ and $U_{\rm s}$ is given by

$$v_f(r_1) = 2\left\langle \varphi'_{1s}(\boldsymbol{r}_3)\left|\frac{1}{r_{13}}\right|\varphi'_{1s}(\boldsymbol{r}_3)\right\rangle. \tag{18}$$

Considering the important contributions from the indirect ionization process, we calculate the cross sections of indirect ionization using the R-matix method,[37] in which the configuration space is divided into two regions at a spherical radius $r = a$. For the boundary of $r < a$, the scattered electron and the target ion with N electrons form a $(N+1)$-electron system, where the $(N+1)$-electron exchange effects are important and must be taken into account. For the boundary of $r > a$, the amplitude of the bound wave function is negligible, and then the exchange interaction between the bound and the continuous electrons can be ignored. For electron-impact ionization of lithium-like ions, the K–L excitation-autoionization process will cause a rapid enhancement of the cross sections at about four times the ionization energy. In present work, the intermediate states $1s2l2l'$ formed by the 1s electron excited to $n = 2$ orbitals are included and partial wave contributions up to angular momentum $L = 7$ are included to obtain converged ionization cross sections, in which the $1s2l2l'\ ^2S^e$, $^2P^o$ resonances dominate the excitation-autoionization contributions.[9,10]

The indirect-ionization cross sections is calculated as

$$\sigma_{EA} = \sum_i \sigma_i^{\rm ex} B_i^A. \tag{19}$$

Here, $\sigma_i^{\rm ex}$ is the electron-impact excitation cross sections and B_i^A is the corresponding branching ratios, represented by $A_{\rm a}/(A_{\rm a}+A_{\rm r})$, $A_{\rm a}$ and $A_{\rm r}$ being the Auger and radiative transition probabilities, respectively.[9,38]

Table 1. Distorting potentials and asymptotic charges by the outgoing electrons in Li-like ions using three models of TPDW00, TPDW01, and TPDW00, respectively.

	Distorting potential		Asymptotic charges	
Model	$U_{\rm p}$	$U_{\rm s}$	$Z_{\rm p}$	$Z_{\rm s}$
TPDW00	$-Z/r_1 + v_i(r_1)$	$-Z/r_2 + v_i(r_2)$	$Z-3$	$Z-3$
TPDW01	$-Z/r_1 + v_i(r_1)$	$-Z/r_2 + v_f(r_2)$	$Z-3$	$Z-2$
TPDW11	$-Z/r_1 + v_f(r_1)$	$-Z/r_2 + v_f(r_2)$	$Z-2$	$Z-2$

2.1. Total cross sections

In the present work, we have calculated the total cross sections of electron-impact ionization for C^{3+}, N^{4+}, O^{5+}, Ne^{7+} and Fe^{23+} ions with incident energies $u_{\rm i}$ in the range of threshold energy units from 1 to 10. The two-potential distorted-wave method is used in the lower energy region, and when the incident energy is above the autoionization threshold, the distorted-wave combined with the R-matrix method is employed to calculate the contributions from the

excitation-autoionization process. The bound-state wavefunctions and ionization energies of Li-like ions are generated from a multi-configuration Dirac–Fock (MCDF) calculation, which is implemented in the relativistic MCDF code written by Desclaux.[39]

One distinct feature of the ionization cross section for lithium-like ions is the important role played by the excitation-autoionization mechanism at the energies between three and five times the direct ionization threshold, which is completely different from the cases of beryllium and boron sequences. For example, this effect contributes approximately 17% of the total ionization cross section of Ne^{7+}, while it is smaller in Ne^{6+} and not observed for Ne^{5+}.[7] In addition, the contribution from the excitation-autoionization process is dominated by $1s2l2l'$ intermediate states. Therefore, the configurations of $1s2s^2$, $1s2s2p$ and $1s2p^2$ are included, where the configurations of $1s2s^2\ ^2S^e$ and $1s2s2p\ ^2P^o$ dominate the excitation-autoionization contributions; the other resonances have minimal contributions to the cross sections.[9,10] The energies and total cross sections are given at autoionization resonance hump in Table 2, along with the other theoretical results and experimental data. Our calculations are close to the experiments and the Coulomb–Born exchange approximation with close-coupling results.[9] Generally, the model TPDW11 is in good agreement with the experimental measurements for the largest difference less than 5%. The only exception is for Ne^{7+} ion, where the TPDW00 model behaves well and there is a 10% discrepancy between TPDW00 and TPDW11 models.

Table 2. Energies E (eV) and total cross sections σ (10^{-3} a.u.) at the positions of autoionization resonances for lithium-like ions.

	Our work				Experiment		Theory	
Ion	E	σ_{01}	σ_{11}	σ_{00}	E	σ	E	σ
C^{3+}	309	109.757	114.954	141.154	312	115.450[a]	306	112.846[d]
N^{4+}	425	52.032	54.150	63.561	420	53.280[b]	431	52.852[d]
O^{5+}	580	27.119	28.078	32.106	590	27.711[b]	572	27.604[d]
Ne^{7+}	920	9.546	9.820	10.852	950	11.427[b]	918	9.856[d]
					921	11.463[c]	917	10.290[e]
Fe^{23+}	6754	0.135	0.136	0.141			6726	0.139 [d]

[a]Ref. [15], [b]Ref. [17], [c]Ref. [7], [d]Ref. [9], [e]Ref. [10].

The total cross sections produced by using the models TPDW00, TPDW01 and TPDW11 for the ions C^{3+}, N^{4+}, O^{5+}, Ne^{7+} and Fe^{23+} are presented in Figs. 1–5, along with available experimental data and theoretical results. Generally the ionization cross section is a slow and smooth varying function of the incident electron energy, but sharp peak appears at about four times the ionization energy. The cross sections using three models appear to be very similar with each other at the low energies, so we present the results in Table 3. The results generated by the TPDW00 model are smaller than TPDW01 and TPDW11 at less than 1.25 times the ionization energy and are larger in higher incident energy. At small incident energies, the model TPDW00 accurately describes continuous electrons because two electrons are screened each other by sharing a small kinetic energy. At large incident energies, the model TPDW01 or TPDW11 is expected to be more reliable, since at least one scattered electron possesses a large kinetic energy, which generates small screening effects. The results of three models become similar as the nuclear charge Z increases because the nuclear potential dominates the cross section of highly charged ions such that the mutual screening effects of continuous electrons affect negligibly. We also present the excitation-autoionization contributions for C^{3+}, N^{4+}, O^{5+}, Ne^{7+} and Fe^{23+} ions from Figs. 1–5. Obviously, the excitation-autoionization mechanism plays a significant role for all the ions. The contributions are approximately 15% of the total cross section at formant in C^{3+}, N^{4+}, O^{5+}, and Ne^{7+} ions, while it is less than 7% for Fe^{23+} ion. Another interesting feature is the shift of the resonant peak toward the lower energy with an increase in the number of nuclear charges. The peak position is about five times the ionization energy for C^{3+} ion, but drops to about three times the ionization energy for Fe^{23+} ion. Note that the cross sections caused by the direct inner-shell ionization are also considered when the incident electron energy is greater than the $1s$ ionization energy threshold, and this contribution never exceeds 15%.

Table 3. The total cross sections σ (10^{-3} a.u.) are calculated for lithium-like ions near the threshold with the models TPDW00, TPDW01 and TPDW11, respectively.

Ion	u_i	σ_{01}	σ_{11}	σ_{00}
C^{3+}	1.1	37.4985	38.0874	35.3090
	1.25	73.2185	75.0885	72.3630
N^{4+}	1.1	16.1024	16.4381	15.3391
	1.25	31.5493	32.4770	31.2827
O^{5+}	1.1	8.0618	8.2331	7.7490
	1.25	15.8234	16.2869	15.7462
Ne^{7+}	1.1	2.6872	2.7398	2.6163
	1.25	5.2893	5.4271	5.2899
Fe^{23+}	1.1	0.0371	0.0374	0.0369
	1.25	0.0735	0.0743	0.0739

Figure 1 shows the total cross sections for C^{3+}, along with the theoretical values[9] and the experimental results[15] with their uncertainty of about 12%. The agreement between the Coulomb–Born exchange results and experiment is good

below 2.5 times the ionization energy. After that, the discrepancy has become more pronounced. As is expected, the TPDW00 model results are much higher than experiment except near the threshold. The TPDW01 or TPDW11 model appears to be somewhat larger compared with the measurements before the peak of direct ionization, with a difference less than 6%. The TPDW11 model is in better agreement with experiment in the autoionization region than Coulomb–Born exchange. Figures 2 and 3 depict the two-potential data for N^{4+} and O^{5+} together with the experimental results,[17] and the theoretical values with the Coulomb–Born exchange method,[9] respectively. Here, the theoretical results containing the excitation-autoionization contributions are discussed. Similarly, the TPDW00 model is higher than experiment, while, this difference becomes smaller with the nuclear charge increasing. The Coulomb–Born exchange approximation is again smaller than our results of two-potential distorted-wave in direct process. However, since the distortion effects will be small at the high energies of autoionization region, the coulomb-wave and distorted-wave results tend to be close. For both ions, the TPDW11 results are in excellent agreement with the experiments.

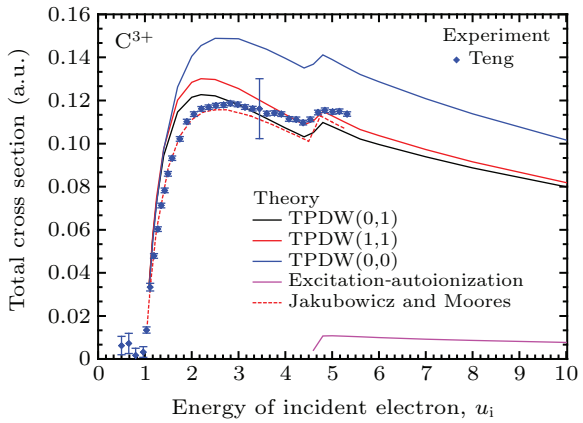


Fig. 1. Electron-impact ionization cross sections of C^{3+} (ionization energy = 64.385 eV). The solid curves represent the two-potential distorted-wave calculations with models TPDW00, TPDW01, and TPDW11 and the results of excitation-autoionization. The Coulomb–Born exchange results[9] with dashed curve and the experimental data[15] with solid dot are shown for comparison.

Figure 4 shows the theoretical results of Ne^{7+}, which include the excitation-autoionization contribution using close-coupling approximation[9] and with the distorted waves-R-matrix method.[10] The Coulomb–Born exchange calculation underestimates the direct ionization contribution below the autoionization threshold, whereas the excitation-autoionization contribution is consistent with the present results. Moreover, the direct ionization cross sections of Riahi *et al.*[10] are lower than others and the excitation-autoionization contributions seem to be overestimated using the R-matrix method. With the nuclear charge increasing, the TPDW00 model is found to be closer to the measurements.[7,17] Our two-potential results provide an excellent estimation for incident energies in the ranging of threshold energy units from 1 to 10.

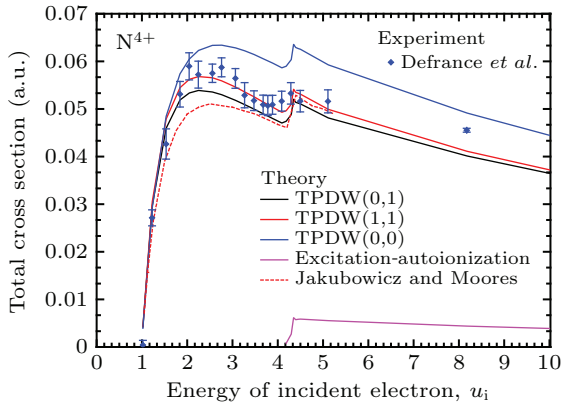


Fig. 2. Electron-impact ionization cross sections of N^{4+} (ionization energy = 97.777 eV). The solid curves represent the two-potential distorted-wave calculations with models TPDW00, TPDW01, and TPDW11 and the results of excitation-autoionization. The Coulomb–Born exchange results[9] with dashed curve and the experimental data[17] with solid dots are shown for comparison.

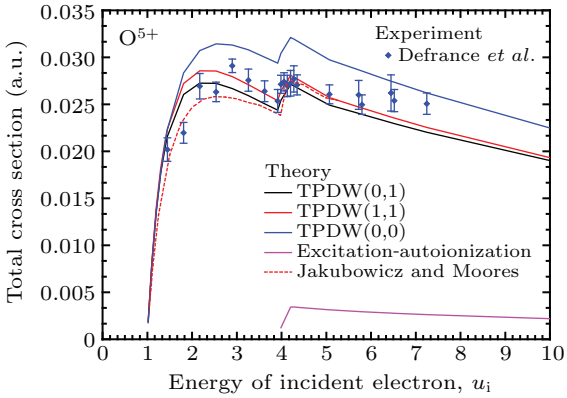


Fig. 3. Electron-impact ionization cross sections of O^{5+} (ionization energy = 138.006 eV). The solid curves represent the two-potential distorted-wave calculations with models TPDW00, TPDW01, and TPDW11 and the results of excitation-autoionization. The Coulomb–Born exchange results[9] with dashed curve and the experimental data[17] with solid dots are shown for comparison.

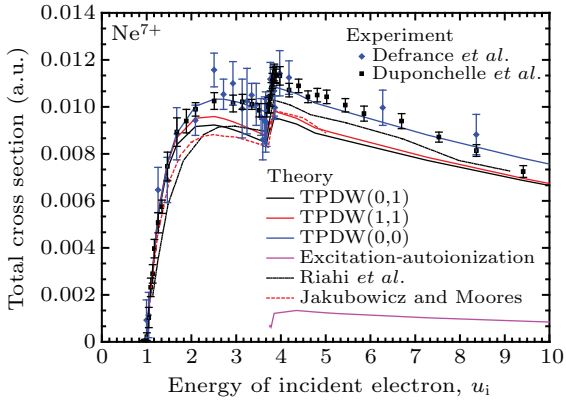


Fig. 4. Electron-impact ionization cross sections of Ne^{7+} (ionization energy = 238.996 eV). The solid curves represent the two-potential distorted-wave calculations with models TPDW00, TPDW01, and TPDW11 and the results of excitation-autoionization. The Coulomb–Born exchange results[9] with dashed curve, the distorted waves-R-matrix results[10] with dotted curve, and the experimental data[7,17] with solid dots are shown for comparison.

Figure 5 shows our data of Fe^{23+} ion, as well as theoretical data[9] and the experiment.[18] Our results are slightly higher than those of Coulomb–Born exchange approximation, in which the relativistic effect is not included. However, the relativistic corrections are important for the case of Fe^{23+} ion. The effect of distortion decreases with increasing charge as expected, and all calculations are more or less consistent.

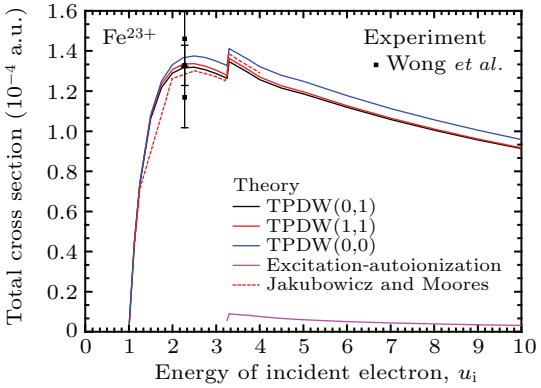


Fig. 5. Electron-impact ionization cross sections of Fe^{23+} (ionization energy = 2046.634 eV). The solid curves represent the two-potential distorted-wave calculations with models TPDW00, TPDW01, and TPDW11 and the results of excitation-autoionization. The Coulomb–Born exchange results[9] with dashed curve and the experimental data[18] with solid dots are shown for comparison.

2.2. Contributions from exchange effect

Since the transition matrix element has been separated into direct, interchange, and capture parts in Eq. (10), we can explore the contributions from different terms in the potential, which is also of great interest in the studies of ionization dynamics. As an example, a separation of the contributions on the total cross sections of C^{3+} and Fe^{23+} ions from model TPDW01 are presented in Fig. 6. Obviously, the direct part plays a major role in both ions. The interchange terms increase the cross sections by 50% near the threshold and decrease them by about 10% after the peak. For C^{3+} ion, the contributions from capture terms are negative and influence on the cross sections is less than 2%. For Fe^{23+}, the trend of the capture terms is similar to the low-Z ions, but the proportion decreases to 0.2%.

It is observed that the capture terms have more contribution for lower-Z ions, but become negligible for higher-Z ions in the selected targets. The bound electrons of lower-Z ions spread wider, so that there is more opportunity for incident electron to overlap and exchange energy with bound electrons. Simultaneously, because the incident electron spends more time to interact with target near the threshold, the exchange effects become more significant. Moreover, the radial integral $\langle W_{\rm pb} R_\lambda W_{\rm si} \rangle$ in the interchange terms[40] become larger; thus the interchange terms contribute significantly near the threshold. However, the bound electrons are more tightly bound together, so there are fewer opportunities to exchange with the incident electron for higher-Z ions.

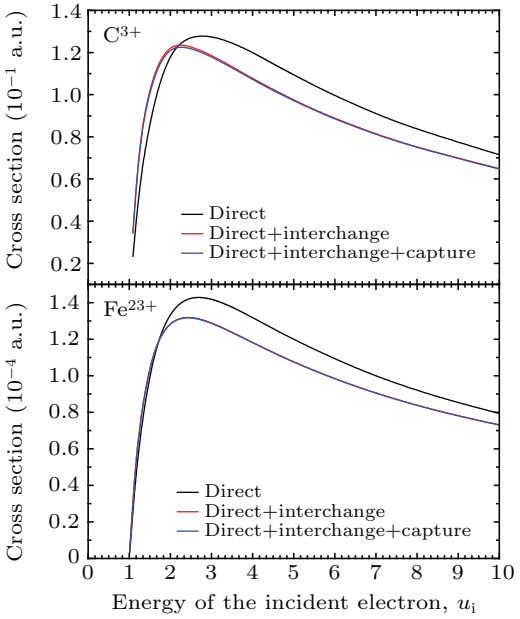


Fig. 6. Contributions from exchange effects on the cross sections of C^{3+} and Fe^{23+} in the model TPDW01.

3. Conclusion

We have applied the two-potential distorted-wave and R-matrix methods to describe the electron-impact ionization with direct and indirect mechanisms for selected lithium-like ions. Several sets of asymptotic charges in three models TPDW00, TPDW01 and TPDW11 are used to characterize the effects of mutual screening from scattered electrons. The total cross sections obtained in the present work for the lithium isoelectronic sequence show good agreement with experimental results. It is found that the model TPDW00 better describes the electron-impact ionization process at lower incident energies, whereas the model TPDW01/TPDW11 works better at higher incident energies. With the nuclear charge increasing, the TPDW00 model becomes more reliable. The contributions from the exchange amplitudes, including the interchange and capture parts, are also discussed in the present work. The interchange term is important for all the isoelectronic sequence and the contribution of capture term only becomes non-negligible for the case of lower-Z ions. Furthermore, the K-L excitation-autoionization processes are non-negligible for lithium-like ions, which contribute at most 7%–15% in the present total cross section calculations. This work can provide a set of high-precision ionization cross section data for related plasma simulations, and it can also provide a reference for future studies with more sophisticated methods.

Acknowledgements

This work is supported by the National Natural Science Foundation of China (Grant Nos. 11934004 and U1832201), the Science Challenge Project (Grant No. TZ2016005), and the CAEP Foundation (Grant No. CX2019022).

References

[1] Mark T D 1992 *Plasma Phys. Contr. F* **34** 2083
[2] Capitelli M, Colonna G, D'Ammando G, Laporta V and Laricchiuta A 2013 *Phys. Plasmas* **20** 101609
[3] Stillman C R, Nilson P M, Ivancic S T, Golovkin I E, Mileham C, Begishev I A and Froula D H 2017 *Phys. Rev. E* **95** 063204
[4] Beiersdorfer P, Brown G V, McKelvey A, Shepherd R, Hoarty D J, Brown C R D, Hill M P, Hobbs L M R, James S F and Morton J and and Wilson L 2019 *Phys. Rev. A* **100** 012511
[5] Alberti A, Munafò A, Koll M, Nishihara M, Pantano C, Freund J B, Elliott G S and Panesi M 2019 *J. Phys. D: Appl. Phys.* **53** 025201
[6] Weber S, Wu Y and Wang J G 2021 *Matter Radiat. Extremes* **6** 023002
[7] Duponchelle M, Khouilid M, Oualim E M, Zhang H and Defrance P 1997 *J. Phys. B: At. Mol. Opt. Phys.* **30** 729
[8] Chen C Y, Yan S X, Teng Z X, Wang Y S, Yang F J and Sun Y S 1998 *J. Phys. B: At. Mol. Opt. Phys.* **31** 2667
[9] Jakubowicz H and Moores D L 1981 *J. Phys. B: At. Mol. Phys.* **14** 3733
[10] Riahi A, Laghdas K, Reid R H G, Rachafi S, Joachain C J and Defrance P 2001 *J. Phys. B: At. Mol. Opt. Phys.* **34** 175
[11] Falk R A and Dunn G H 1983 *Phys. Rev. A* **27** 754
[12] Woitke O, Djurić N, Dunn G H, Bannister M E, Smith A C H, Wallbank B, Badnell N R and Pindzola M S 1998 *Phys. Rev. A* **58** 4512
[13] Crandall D H, Phaneuf R A, Hasselquist B E and Gregory D C 1979 *J. Phys. B: At. Mol. Phys.* **12** L249
[14] Crandall D H, Phaneuf R A, Gregory D C, Howald A M, Mueller D W, Morgan T J, Dunn G H, Griffin D C and Henry R J W 1986 *Phys. Rev. A* **34** 1757
[15] Teng H, Knopp H, Ricz S, Schippers S, Berrington K A and Müller A 2000 *Phys. Rev. A* **61** 060704
[16] Kunc J A 1980 *J. Phys. B: At. Mol. Phys.* **13** 587
[17] Defrance P, Chantrenne S, Rachafi S, Belic D S, Jureta J, Gregory D and Brouillard F 1990 *J. Phys. B: At. Mol. Opt. Phys.* **23** 2333
[18] Wong K L, Beiersdorfer P, Chen M H, Marrs R E, Reed K J, Scofield J H, Vogel D A and Zasadzinski R 1993 *Phys. Rev. A* **48** 2850
[19] Wong K L, Beiersdorfer P, Vogel D, Marrs R and Levine M 1991 *Z. Phys. D: At. Mol. Clusters* **21** S197
[20] Claytor N, Feinberg B, Gould H, Bemis J, Curtis E, Campo J G, Ludemann C A and Vane C R 1988 *Phys. Rev. Lett.* **61** 2081
[21] Rudge M R H 1968 *Rev. Mod. Phys.* **40** 564
[22] Younger S M 1980 *Phys. Rev. A* **22** 111
[23] Younger S M 1981 *J. Quant. Spectrosc. Radiat. Transfer* **26** 329
[24] Fursa D V and Bray I 1997 *J. Phys. B: At. Mol. Phys.* **30** 757
[25] Bartschat K and Burke P G 1987 *Phys. B: At. Mol. Phys.* **20** 3191
[26] Huang K N 1983 *Phys. Rev. A* **28** 1869
[27] Kao H C, Kuo T Y, Yen H P, Wei C M and Huang K N 1992 *Phys. Rev. A* **45** 4646
[28] Hsu S W, Kuo T Y, Chen C M J and Huang K N 1992 *Phys. Lett. A* **167** 277
[29] Kuo T Y, Chen C M J, Hsu S W and Huang K N 1993 *Phys. Rev. A* **48** 357
[30] Chang J C, Wei C M, Kuo T Y and Huang K N 1994 *J. Phys. B: At. Mol. Opt. Phys.* **27** 4715
[31] Kuo T Y and Huang K N 2001 *Phys. Rev. A* **64** 062711
[32] Kuo T Y and Huang K N 2001 *Phys. Rev. A* **64** 032710
[33] Kuo T Y and Huang K N 2003 *J. Phys. B: At. Mol. Opt. Phys.* **36** 353
[34] Chang J C, Sun H L, Cheng W Y and Huang K N 2004 *Phys. Rev. A* **69** 052713
[35] Norrington P H and Grant I P 1987 *J. Phys. B: At. Mol. Phys.* **20** 4869
[36] Ait-Tahar S, Grant I P and Norrington P H 1996 *Phys. Rev. A* **54** 3984
[37] Chang J J 1977 *J. Phys. B: At. Mol. Phys.* **10** 3335
[38] Reed K J and Chen M H 1992 *Phys. Rev. A* **45** 4519
[39] Desclaux J P 1975 *Comput. Phys. Commun.* **9** 31
[40] Sun H L, Chang J C, Hsiao J T, Lin S F and Huang K N 2010 *Phys. Rev. A* **4** 81